

Nanostructured BiVO₄ Photoanodes Fabricated by Vanadium-infused Interaction for Efficient Solar Water Splitting

Amar K. Salih^{1,2}, Abdul Zeeshan Khan³, Qasem A. Drmosh⁴, Tarek A. Kandiel^{3,4*}, Mohammad Qamar⁴, Tahir Naveed Jahangir³, Cuong Ton-That^{1,*}, Zain H. Yamani^{2,4}

¹School of Mathematical and Physical Sciences, University of Technology Sydney, Ultimo, New South Wales 2007, Australia

²Physics Department, King Fahd University of Petroleum and Minerals, Dhahran, 31261, Saudi Arabia

³Chemistry Department, King Fahd University of Petroleum and Minerals, Dhahran, 31261, Saudi Arabia

⁴Center of Hydrogen and Energy Storage (IRC-HES), King Fahd University of Petroleum and Minerals, Dhahran 31261, Saudi Arabia

*Corresponding authors.

E-mail address: Cuong.Ton-That@uts.edu.au ; tarek.kandiel@kfupm.edu.sa

ABSTRACT

Bismuth vanadate (BiVO₄) has emerged as a highly prospective material for photoanodes in photoelectrochemical (PEC) water oxidation. However, current limitations with this material lie in the difficulties in producing stable and continuous BiVO₄ layers with efficient carrier transfer kinetics, thereby impeding its widespread application in water splitting processes. This study introduces a new fabrication approach that yields continuous, monoclinic nanostructured BiVO₄ films, paving the way for their use as photoanodes in efficient PEC water oxidation for hydrogen production under solar light conditions. The fabrication involves the intercalation of vanadium (V) ions into Bi₂O₃ films at 450°C. Upon interaction with V ions, the film undergoes a transformation from tetragonal Bi₂O₃ to monoclinic scheelite BiVO₄. This synthesis method enables the fabrication of single monoclinic phase BiVO₄ films with thicknesses up to 270 nm. The engineered monoclinic BiVO₄ film, devoid of any pinholes that could cause carrier loss, exhibits a robust photocurrent of 1.0 mA/cm² at 1.23 V_{RHE} in a neutral electrolyte, without requiring additional

modifications or doping. Moreover, we demonstrate that the incorporation of a cobalt phosphate (Co–Pi) co-catalyst into the BiVO₄ photoanode significantly enhances the lifetime of photogenerated holes by a factor of nine, resulting in a further elevation of the photocurrent to 2.9 mA/cm². This remarkable PEC enhancement can be attributed to the surface state passivation by the Co–Pi co-catalyst. Our fabrication approach opens up a new facile route for producing large-scale, highly efficient BiVO₄ photoanodes for PEC water splitting technology.

Keywords: photoelectrochemical water splitting; BiVO₄; photoanodes; vanadium intercalation; Co–Pi co-catalyst

1. Introduction

Solar energy conversion to electrochemical energy offers a viable avenue for producing hydrogen through the photoelectrochemical (PEC) water splitting process.¹ This PEC process heavily relies on suitable semiconductor photoanodes that can facilitate efficient light absorption and fast charge transport at the semiconductor/electrolyte interface (SEI). Metal oxide semiconductors such as ZnO, WO₃, Fe₂O₃, TiO₂, and BiVO₄ are promising candidates for practical PEC water oxidation owing to their facile preparation, low fabrication cost and photo-oxidative capability.^{2, 3} Among these oxides, monoclinic BiVO₄ stands out due to its narrow bandgap of 2.4 eV and a favorable valence band edge position for oxygen evolution. These characteristics enable efficient water oxidation with a recently reported solar-to-hydrogen (STH) efficiency of 9.2%.⁴⁻⁶

BiVO₄ photoanodes have been theoretically predicted to achieve 7.5 mA/cm² at 1.23 V_{RHE} (voltage with respect to reversible hydrogen electrode) under AM1.5 G illumination (100 mW/cm²);⁷ however, experimentally reported photocurrent densities fall well below this anticipated value. This disparity primarily arises from the low utilization of photogenerated electron-hole pairs in the PEC processes. Extensive research efforts have been devoted to improving water oxidation efficiency through the optimization of various BiVO₄ fabrication techniques. Presently, BiVO₄ films are commonly produced using physical vapor deposition, which offers advantages such as uniformity, large photoanodes, and adjustable film thickness. However, this method typically produces structure-less films with limited surface areas available for the photo-oxidative reaction, leading to low water oxidation efficiencies. Photocurrents in the range of 0.01–0.5 mA/cm² at 1.23 V_{RHE} are typically achieved even after fine-tuning the deposition parameters of BiVO₄ photoanodes or employing co-sputtering of Bi₂O₃ and V targets.⁸⁻¹⁰ Conversely, chemical fabrication methods can yield nanostructured films with a high specific surface area for BiVO₄

photoanodes. However, a major drawback of these methods is the formation of a discontinuous BiVO_4 layer,¹¹⁻¹⁴ which can lead to significant PEC efficiency loss due to solution-mediated reduction of photogenerated carriers.¹⁵ Figure 1 illustrates the primary pathways of carrier loss on BiVO_4 photoanodes deposited on a typical fluorine-doped tin oxide (FTO) substrate. The water oxidation process is inherently slow, which allows photogenerated holes to recombine with electrons before participating in the oxidation reaction. This recombination commonly occurs at defects within the bulk of the BiVO_4 film (process a) or on its surface (process b). Additionally, back reduction of the oxidation products and electron back injection through solution-mediated recombination at voids or exposed regions of the film (process c) have been identified as substantial carrier loss mechanisms.^{15, 16} These pathways collectively limit the efficiency and stability of BiVO_4 photoanodes in water splitting applications. Addressing these challenges is imperative for enhancing the performance of BiVO_4 -based water splitting systems.

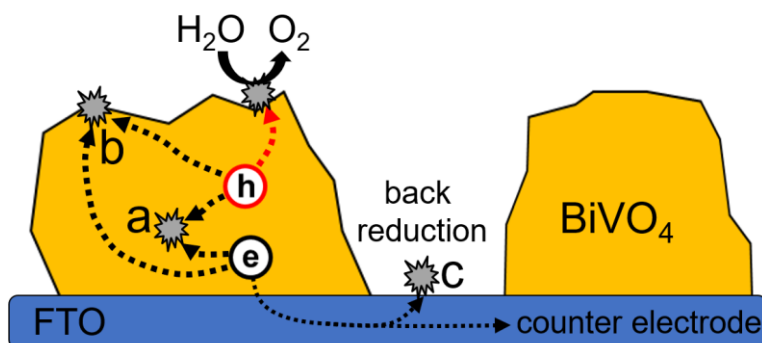


Figure 1. Schematic illustrating the primary reaction pathways responsible for the decline in PEC efficiency in water oxidation. Three main routes are: electron-hole recombination at bulk defects (process a) or surface defects (b), and solution-mediated back reduction occurring through exposed regions of the FTO substrate (c). Arrows show the trajectories of electrons and holes through the BiVO_4 film and FTO substrate.

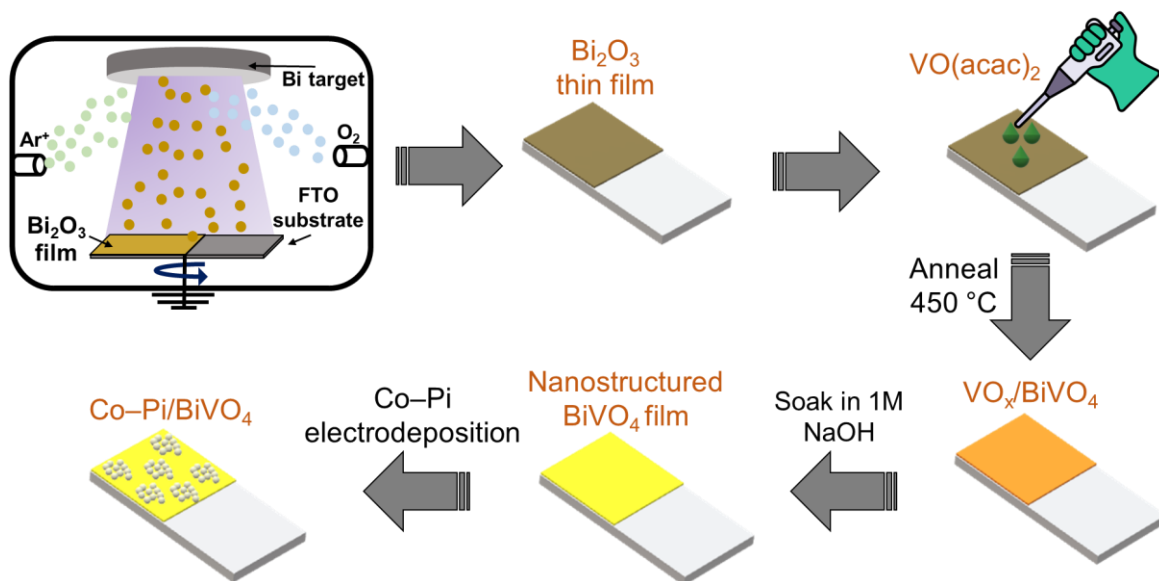
This work presents a new method for fabricating continuous, nanostructured BiVO₄ films without pinholes, establishing them as highly efficient photoanodes for PEC water oxidation in hydrogen production. The BiVO₄ photoanode in the monoclinic scheelite phase is fabricated by intercalating vanadium (V) ions into a sputtered Bi₂O₃ film at 450 °C. The analysis evaluates the quality of the intercalated films and their PEC performance over film thicknesses from 60 to 1100 nm. The optimized BiVO₄ photoanode in this fabrication approach is shown to exhibit an exceptional and stable photocurrent density of up to 1.0 mA/cm² under neutral pH and in the absence of a hole scavenger. The outstanding performance of the BiVO₄ photoanode arises from the elimination of solution-mediated recombination through exposed FTO regions (process c) and the optimization of the charge transfer path through the photoanode thickness. Moreover, we demonstrate that the incorporation of cobalt phosphate (Co–Pi) catalyst can effectively suppress surface recombination (process b) and extend the lifetime of photogenerated holes by nine times, resulting in an outstanding photocurrent up to 2.9 mA/cm² at 1.23 V_{RHE}.

2. Experimental Details

2.1 Preparation of BiVO₄ films

BiVO₄ and Co–Pi/BiVO₄ films were fabricated through a process involving V intercalation and Co–Pi electrodeposition, as illustrated in Scheme 1. Bi₂O₃ films, with thickness ranging from 60 to 1100 nm, were deposited on the FTO substrate (8 Ω/sq resistivity, from Sigma-Aldrich), with a geometrical area of 1.0 cm², using metallic Bi target (99.995% purity) and a direct current (DC) reactive sputtering magnetron (Nanomaster, NSC-4000). Throughout the deposition process, the chamber's base pressure remained at 9×10^{-6} torr, and the working pressure was maintained at 3×10^{-3} torr within an atmosphere of oxygen and argon gases (1:1 ratio of oxygen to argon). The thickness of the Bi₂O₃ films was controlled by adjusting the deposition time. Following this, 30

μL of a solution containing 0.15 M vanadyl acetylacetonate ($\text{C}_{10}\text{H}_{14}\text{O}_5\text{V}$, $\text{VO}(\text{acac})_2$) dissolved in $\text{C}_2\text{H}_6\text{OS}$ was drop-casted onto the Bi_2O_3 film surface. The films were then annealed for 2 hours at $450\text{ }^\circ\text{C}$ (ramping rate of $2\text{ }^\circ\text{C}/\text{min}$) in an ambient atmosphere. At this temperature, the decomposition of $\text{VO}(\text{acac})_2$ led to the production of VO_x species,¹⁷ facilitating their diffusion into the Bi_2O_3 film. The intercalated film was subsequently agitated in a 1.0 M NaOH solution for 10 min to remove any excess of VO_x on the surface. To further enhance the PEC performance, the BiVO_4 films were modified with a Co–Pi co-catalyst using photo-assisted electrochemical deposition. This deposition was conducted at $1.6\text{ V}_{\text{RHE}}$ for 3 minutes using 0.5 mM $\text{Co}(\text{NO}_3)_2$ in 0.1 M $\text{H}_2\text{KO}_4\text{P}$ (phosphate-buffered saline, PBS) solution with the pH maintained at 7.



Scheme 1. Schematic illustration of the fabrication steps for BiVO_4 and Co-Pi/BiVO_4 photoanodes.

2.2 Structural and PEC characterization

X-ray diffraction (XRD) analysis was carried out using a Rigaku Miniflex 600 X-ray Diffractometer. An Agilent Cary 5000 UV-Vis-NIR spectrometer, operating in transmission mode,

was employed to assess the optical properties of the films. Film surface morphology and cross-sections were examined using Tescan Lyra-3 field emission scanning electron microscopy (FE-SEM). Chemical analysis via X-ray photoelectron spectroscopy (XPS) was performed using the ESCALAB250Xi Thermo Fisher spectrometer.

Photoelectrochemical (PEC) performance was tested in a three-electrode configuration using an Autolab potentiostat (PGSTAT 302N). The intercalated BiVO₄ films were used as the working electrode, while a Pt coil and Ag/AgCl (3.0 KCl) were used as the counter and reference electrodes, respectively. A neutral solution of 0.5 M PBS was used as an electrolyte in a homemade cell with a quartz window. To investigate the impact of hole scavengers on PEC performance, 0.5 M PBS + 0.5 M Na₂SO₃ aqueous solution was used as an electrolyte to minimize surface electron-hole pair recombination on the BiVO₄ photoanode.¹⁸ A solar simulator 1002 SunLite was used to simulate solar conditions with a light intensity of 100 mW/cm². The reversible hydrogen electrode potential (E_{RHE}) was calculated from the applied potential ($E_{Ag/AgCl}$) using the Nernst equation:¹⁹

$$E_{RHE} = E_{Ag/AgCl} + 0.0591 \cdot pH + E_{Ag/AgCl}^o \quad \text{Eq. (1)}$$

where $E_{Ag/AgCl}^o$ is the standard electrode potential, which is 0.198 V. The chronoamperometry response for the photoanode was recorded to calculate the incident photon to current efficiency (IPCE) at 1.23 V_{RHE}. Collimated monochromatic LED light sources (Thorlabs) with wavelengths between 375 to 565 nm were used, and light intensity was calibrated using an FDS100-CAL photodiode. For the photoelectrochemical impedance spectroscopy (PEIS), the same Autolab potentiostat setup was employed. Nyquist plots were measured at a biased potential of 0.6 V_{RHE} over the frequency range from 100 kHz to 0.1 Hz. Finally, Mott-Schottky analysis was performed

at 10 kHz in a potential window from 0.3 – 1.4 V_{RHE} under dark conditions, and only the linear part of the $1/C^2$ versus potential plot was considered.

3. Results and discussion

3.1 Structural, morphological, optical, and compositional analyses

Fig. 2(a) presents the XRD patterns of both V-intercalated BiVO₄ and Bi₂O₃ films for comparison. Detailed XRD analysis, including the indexation of all diffraction peaks in the BiVO₄ and Bi₂O₃ films with thicknesses ranging from 60 to 1100 nm, is provided in Fig. S1(a). The Bi₂O₃ film exhibits dominant XRD peaks corresponding to (220), (013), and (123) reflections of the tetragonal crystal structure. Upon V intercalation into the 60-nm and 270-nm thick films, these Bi₂O₃ peaks completely disappear, indicating a complete phase transformation into monoclinic scheelite BiVO₄. The V-intercalated BiVO₄ films all display clearly identifiable peaks (011), (121), (040), (211) and (161) of the monoclinic phase (JCPDS no. 14–0688); however, residual Bi₂O₃ tetragonal phase is observed in 520, 800, and 1100 nm thick films, likely due to incomplete diffusion of V ions into these thick Bi₂O₃ films. No distinct Co–Pi XRD peaks are detectable in the BiVO₄ film after the deposition of the Co–Pi catalyst [Figure S1(b)]. XPS analysis of the V-intercalated BiVO₄ films, presented in Fig. S2, confirms the formation of BiVO₄ after the V intercalation, with the presence of anticipated photoemission signatures corresponding to Bi, V, and O. The strong V 2p XPS signal after Ar⁺ ions etching for 120 seconds provides further support that V ions are incorporated throughout the thickness of the film, extending down to the substrate. The Bi 4f spectrum reveals a doublet-peak consisting of Bi 4f_{7/2} and 4f_{5/2} components at the binding energies of 158.6 eV and 164.0 eV, consistent with reported values for with BiVO₄.²⁰ Furthermore, the

successful incorporation of the Co–Pi catalyst on the film surface is confirmed by the Co 2p and P 2p XPS spectra in Fig. S2(e, f).

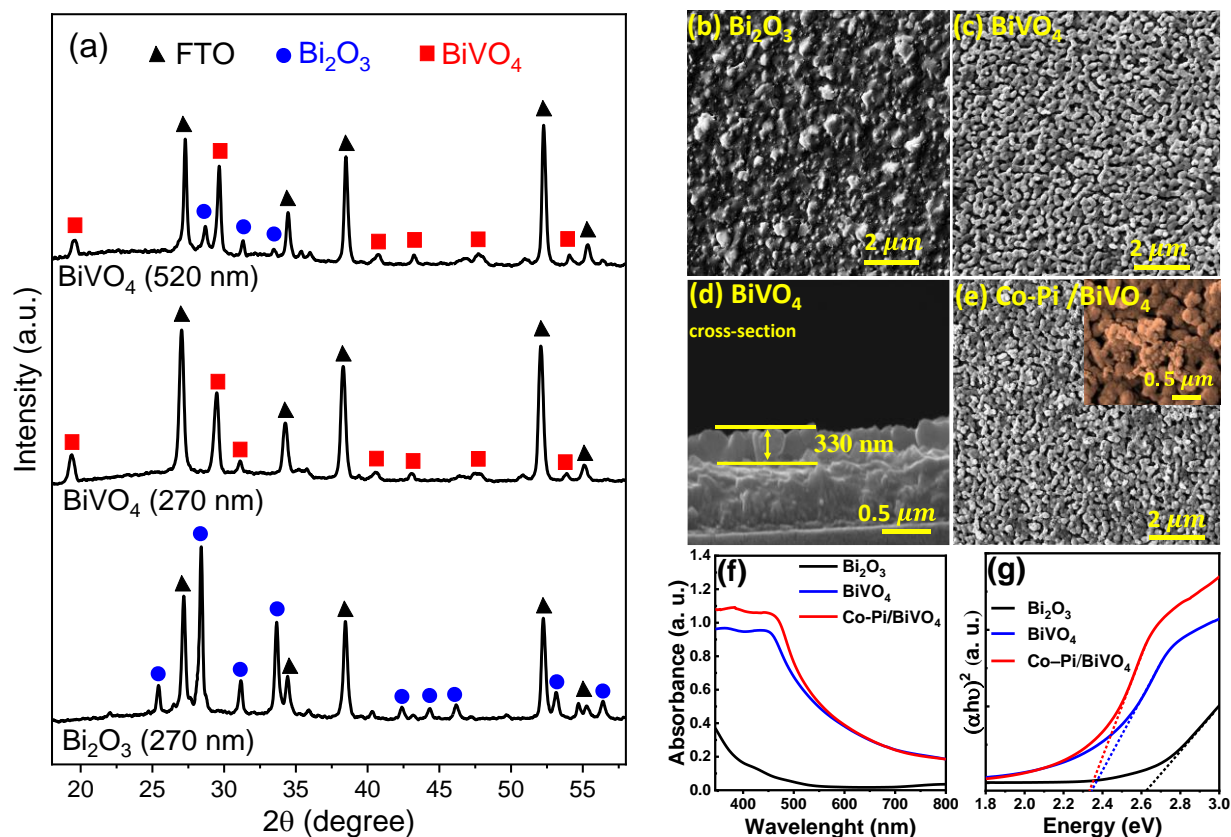


Figure 2. (a) XRD patterns of BiVO₄ and Bi₂O₃ films with thicknesses of 270 nm and 520 nm. Black triangles represent the FTO substrate, while blue circles and red squares indicate reflections from tetragonal Bi₂O₃ and monoclinic BiVO₄ phases, respectively. Complete phase transition to monoclinic BiVO₄ occurs in 270-nm thick film, while a residual Bi₂O₃ phase is present in the 520-nm thick film. (b-e) SEM images of the 270-nm Bi₂O₃ film, its corresponding BiVO₄, and Co–Pi/BiVO₄ films. Both BiVO₄ and Co–Pi/BiVO₄ films exhibit continuous, nanostructured morphology. (f) Optical absorbance spectra of Bi₂O₃, BiVO₄, and Co–Pi/BiVO₄ films showing an ~ 80% increase in optical absorption at wavelengths below 500 nm after the transformation to BiVO₄, while the Co–Pi deposition induces marginal absorption rise. (g) Tauc plots yielding $E_g = 2.64 \pm 0.05$ eV for Bi₂O₃ and $E_g = 2.36 \pm 0.03$ eV for BiVO₄ and Co–Pi/BiVO₄ films.

The surface morphology of a typical 270 nm Bi_2O_3 film and corresponding BiVO_4 film after the V intercalation are displayed in the top-view and cross-section SEM images in Fig. 2(b-e). The initial Bi_2O_3 film exhibits a rough, island-like surface structure. However, following the V intercalation, the film is transformed into a continuous, nanostructured BiVO_4 film with no discernible pinholes. The BiVO_4 film has a granular surface texture, characterized by densely packed grains with diameters of about 100 nm. This pinhole-free and nanostructured nature, coupled with the achievement of a pure monoclinic phase in the BiVO_4 film, plays a crucial role in enhancing the PEC oxidation efficiency, as discussed above. Notably, the thickness of the BiVO_4 film increases slightly from 270 to 330 nm following the V incorporation, as shown in Fig. 2(d). The SEM image of the Co-Pi/ BiVO_4 film in Fig. 2(e) reveals the presence of Co-Pi catalyst nanoparticles with diameters of $\sim 30 - 50$ nm on the film surface. Notably, the film morphology remains unaffected by the Co-Pi electrodeposition process. The energy dispersive X-ray (EDX) spectrum of the Co-Pi/ BiVO_4 film and the SEM image of Co-Pi nanoparticles, presented in Fig. S3, confirm the successful deposition of the Co-Pi particles onto the BiVO_4 film. Upon the V intercalation, the film exhibits a substantial increase of approximately 80% in optical absorption at wavelengths below 500 nm compared to the Bi_2O_3 film, as shown in Figure 2(f), consistent with the formation of monoclinic BiVO_4 . The addition of Co-Pi co-catalyst does not result in any noticeable impact on the optical absorption of the film. The optical bandgap (E_g) of the films, determined using the Tauc plot in Fig. 2(g), is $E_g = 2.64 \text{ eV} \pm 0.05 \text{ eV}$ for the Bi_2O_3 film and $E_g = 2.36 \pm 0.03 \text{ eV}$ for the BiVO_4 and Co-Pi/ BiVO_4 films; the latter value is in agreement with the bandgap of monoclinic BiVO_4 .²¹ The optical transmission spectrum of the BiVO_4 film, presented in Figure S4, shows a transmittance of $< 10\%$ for wavelengths below 450 nm and a broad edge that allows this film to absorb well into the visible range.

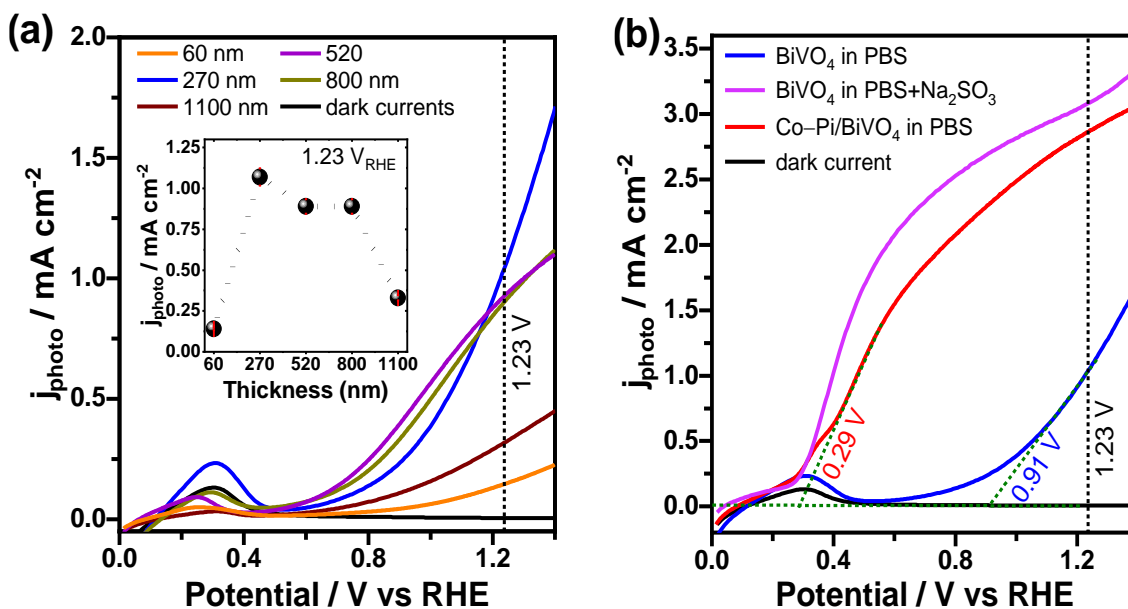
3.2 Photoelectrochemical water splitting performance

The linear sweep voltammetry (LSV) characteristics of the intercalated BiVO₄ in Fig. 3(a) show an increase in current density under illumination, with zero current in the dark. The observed photocurrent peak at around 0.3 V_{RHE} is associated with the redox transition between V⁴⁺ and V⁵⁺ states within BiVO₄ photoanodes.²² The BiVO₄ film ($t = 60$ nm) exhibits a relatively low photocurrent (0.15 mA/cm² at 1.23 V_{RHE}), likely due to its low thickness and reduced crystallinity; these factors contribute to diminished light absorption and increased charge carrier scattering.²³ The BiVO₄ photoanode ($t = 270$ nm) exhibits the highest PEC performance, with a photocurrent density of 1.0 mA/cm² at 1.23 V_{RHE}, measured under neutral pH and in the absence of a hole scavenger. This level of photocurrent ranks among the highest reported for uncatalyzed BiVO₄ photoanodes recorded under comparable conditions, as summarized in Table S1. The excellent PEC performance is attributed to the high film quality achieved through our new fabrication approach. The BiVO₄ photoanodes with greater Bi₂O₃ thicknesses ($t = 520, 800,$ and 1100 nm) exhibit lower photocurrent densities, as shown in the inset of Fig. 3(a). In these thicker films, the possible formation of a BiVO₄/Bi₂O₃ heterojunction could cause holes in the BiVO₄ layer to migrate towards the underlying Bi₂O₃ layer due to the band alignment and the built-in electric field at the heterojunction interface, consequently reducing the availability of holes for water oxidation.²⁴ Another factor contributing to the lower photocurrent densities in the thick films could be an increased film resistance, thus constraining the availability of photogenerated holes at the BiVO₄ surface.^{25, 26} Fig. 3(b) presents an LSV comparison between the BiVO₄ and Co–Pi/BiVO₄ photoanodes in PBS electrolyte, alongside the BiVO₄ photoanode in PBS + Na₂SO₃ electrolyte. The comparison reveals an increase in the optimum BiVO₄ photocurrent to around 3.1 mA/cm² at 1.23 V_{RHE} after the addition of the hole scavenger Na₂SO₃. This suggests a heightened frequency

of SO_3^{2-} oxidation by photogenerated holes on the BiVO_4 surface, compared with the water oxidation process.²⁷ Furthermore, in comparison to other BiVO_4 electrodes synthesized via chemical fabrication methods,^{28,29} the photocurrent attained during the hole-scavenger test by this BiVO_4 photoanode is notably higher (3.1 mA/cm^2). This observation suggests an effective suppression of charge recombination that may occur at the exposed areas of the substrate (see Figure 1). Following the Co–Pi incorporation into the optimized BiVO_4 photoanode, the photocurrent reaches 2.9 mA/cm^2 at $1.23 \text{ V}_{\text{RHE}}$, with an onset potential of $0.25 \text{ V}_{\text{RHE}}$; this performance closely approaches the level achieved with the hole scavenger [Fig. 3(b)]. The enhanced photocurrent can be attributed to holes in the valence band of BiVO_4 transferring to the Co–Pi co-catalyst, where they participate in the oxidation of Co^{2+} ions to Co^{3+} and potentially further to Co^{4+} , which are the highly active species driving the water oxidation.³⁰ The onset potential of the photoanodes, determined from the linear extrapolation of LSV curves, is 0.91 and 0.29 V for BiVO_4 and Co–Pi/ BiVO_4 , respectively. This large cathodic shift indicates diminished surface charge recombination facilitated by the Co–Pi co-catalyst. Further analysis of the LSV curves obtained for the BiVO_4 and Co–Pi/ BiVO_4 photoanodes under chopped light illumination (Fig. S5) reveal diminished anodic spikes with increasing applied potential. This observation suggests that the applied positive potential effectively diminishes electron concentration from surface states, thereby minimizing charge recombination and simultaneously enhancing the kinetics of hole transfer at the SEI during the water oxidation process.

The stability of the BiVO_4 and Co–Pi/ BiVO_4 photoanodes was examined over a 2-hour duration, as depicted in Fig. 3(c). The results reveal that the virtually unchanged photocurrent at 1.0 mA/cm^2 during this period. However, for the Co–Pi/ BiVO_4 photoanode, the photocurrent gradually decreases from 2.9 to 2.5 mA/cm^2 after 2 hours. This decline is attributed to the generation of high

photocurrent, causing partial blockage of the electrode surface due to continuous bubble formation. Chopped light chronoamperometry was also conducted for the BiVO₄ and Co–Pi/BiVO₄ photoanodes at 1.23 V_{RHE} under standard illumination conditions, as shown in Fig. 3(d). The consistent photocurrents observed during the cycles of light-on and light-off for these photoanodes confirm their fast photo-response and highly stable photocurrent. Furthermore, the anodic spike after sudden illumination for the Co–Pi/BiVO₄ photoanode is considerably higher than for BiVO₄, indicating a greater accumulation of holes on the Co–Pi/BiVO₄ surface compared to the bare BiVO₄ surface.



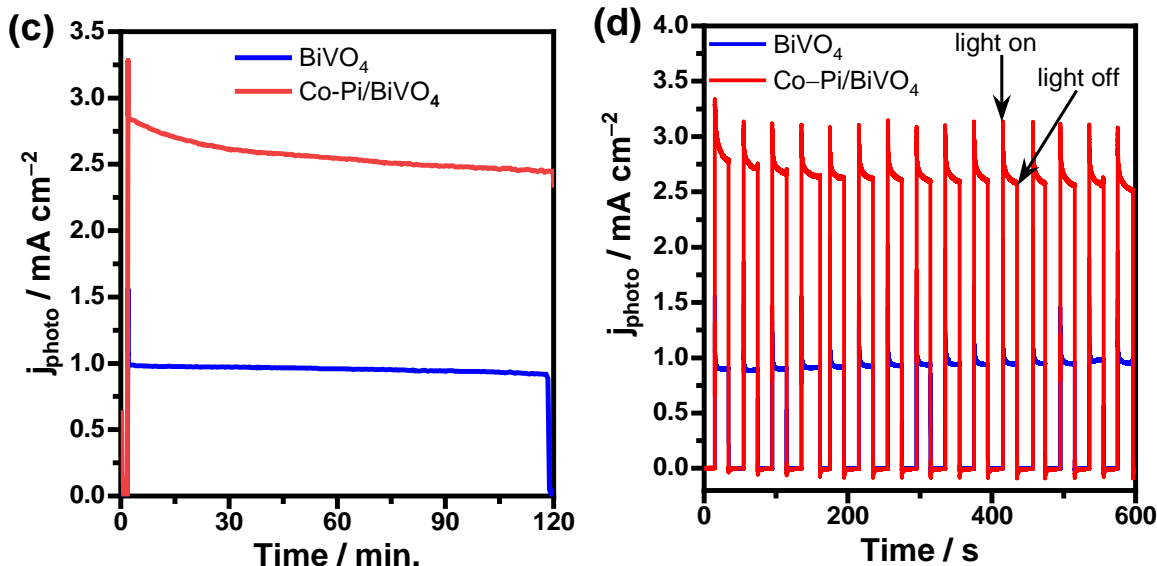


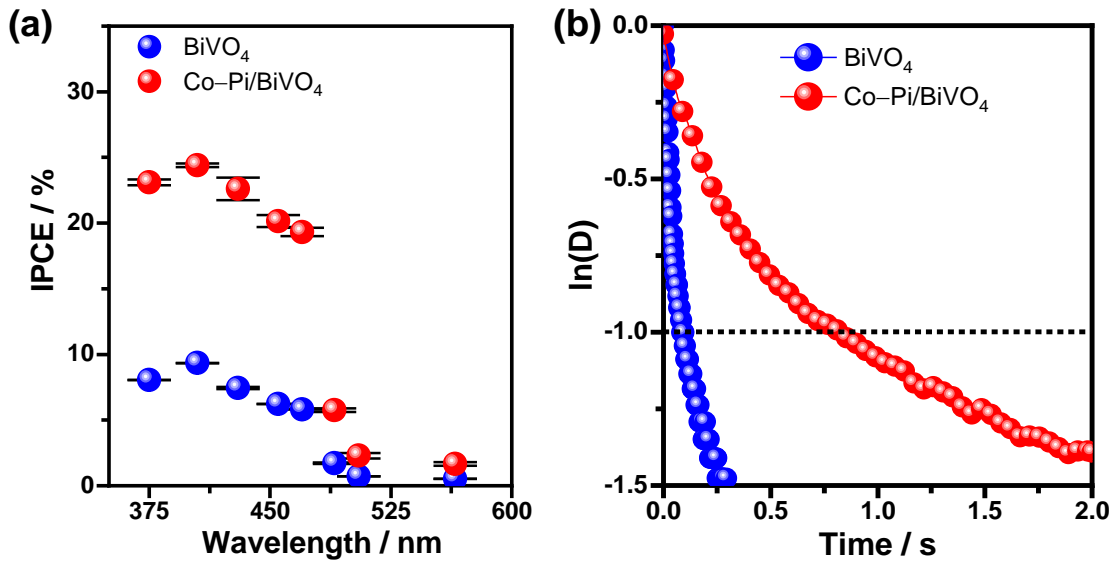
Figure 3. (a) LSV curves of the BiVO_4 photoanodes derived from Bi_2O_3 films with varying thicknesses between 60 and 1100 nm. The inset shows the highest photocurrent of 1.0 mA/cm^2 at 1.23 V_{RHE} for the 270 nm thick photoanode. (b) LSV curves of the BiVO_4 and Co-Pi/BiVO_4 photoanodes in PBS electrolyte, and BiVO_4 photoanode in PBS + Na_2SO_3 electrolyte. After Co-Pi loading, the photocurrent increases from around 1.0 to 2.9 mA cm^{-2} at 1.23 V_{RHE} . (c) Endurance testing performed on BiVO_4 and Co-Pi/BiVO_4 photoanodes, demonstrating significant stability over 2 hours of continuous illumination. (d) Chopped light stability testing for the photoanodes, revealing consistent and fast responses during light modulation, with no electro-current detected in the absence of light.

The performance of the intercalated BiVO_4 photoanode was further examined via incident photon-to-current efficiency (IPCE) across the wavelength range from 375 to 565 nm, as shown in Fig. 4(a). The IPCE of the BiVO_4 photoanode reaches approximately 9% at 405 nm, which is higher than reported values of 3% deposited BiVO_4 films.^{28, 31} The significant increase in the IPCE value is attributed to the uniformity of the BiVO_4 film and complete coverage of the FTO substrate, reducing the carrier loss due to back reduction as illustrated in Fig. 1. As expected, the IPCE increases to ~ 25% after the addition of the Co-Pi co-catalyst, which is consistent with the LSV results in Fig 3(b). The transient photocurrent (TPC) shows that both BiVO_4 and Co-Pi/BiVO_4 photoanodes exhibit anodic and cathodic photocurrent spikes, as shown in Fig. S6. The anodic

spike (I_m) is observed following sudden illumination, resulting from the accumulation of holes on surface states and ultimately reaching a stable photocurrent (I_s). The transient decay time (τ) of the Co–Pi/BiVO₄ and BiVO₄ photoanodes is evaluated to gain further insights into the lifetime of the trapped holes. A parameter D is calculated from the TPC response using:³²

$$D = \frac{I_t - I_s}{I_m - I_s} \quad \text{Eq. (2)}$$

where I_t is the time-dependent photocurrent. The decay time, determined from the plot of $\ln(D)$ versus t shown in Fig. 4(b), is found to be $\tau = 0.10 \pm 0.01$ and 0.90 ± 0.05 s for the BiVO₄ and Co–Pi/BiVO₄ photoanodes, respectively. This nine-fold increase in the decay time for the Co–Pi/BiVO₄ photoanode indicates photogenerated holes remain available much longer (9 times longer) for water oxidation. Such a prolonged lifetime of photogenerated holes can be attributed to the passivation of BiVO₄ surface states by Co–Pi.



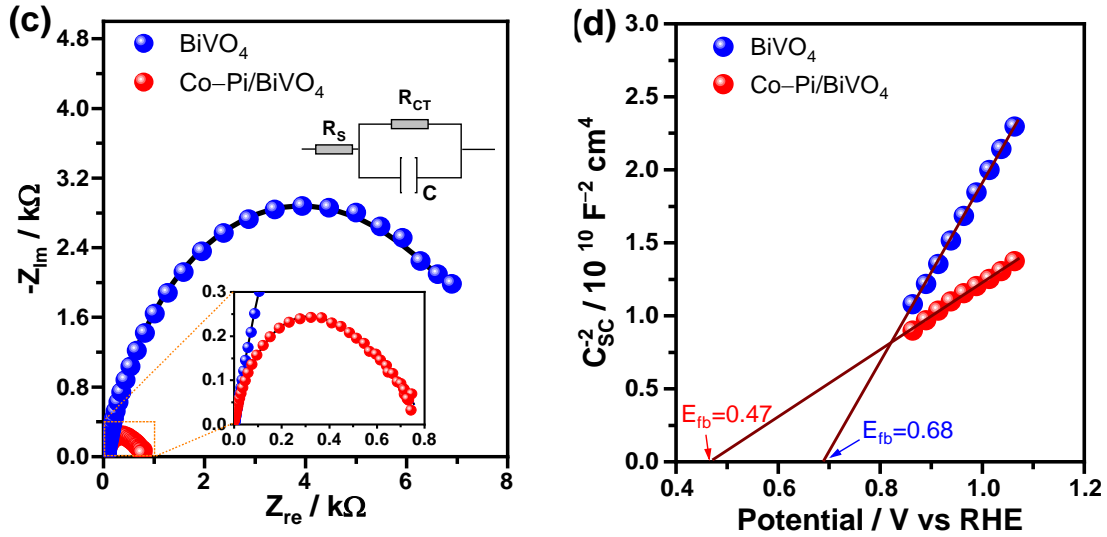


Figure 4. (a) IPCE for BiVO₄ and Co–Pi/BiVO₄ photoanodes measured at various wavelengths between 375 and 565 nm. The black lines indicate estimated uncertainties. (b) Plot of $\ln(D)$ versus time for the photoanodes, yielding $\tau = 0.10 \pm 0.01$ and 0.90 ± 0.05 s for BiVO₄ and Co–Pi/BiVO₄, respectively, indicating a remarkable enhancement in hole lifetime due to surface passivation by Co–Pi. (c) Nyquist plots and the equivalent circuit model (inset) for the BiVO₄ and Co–Pi/BiVO₄ photoanodes at $0.6 V_{\text{RHE}}$. (d) Mott-Schottky plots for the photoanodes under dark conditions. The positive slope indicates *n*-type characteristics, with a cathodic shift of E_{fb} by $-0.21 V_{\text{RHE}}$.

The PEIS method was used to investigate the charge transfer kinetics in the electrodes, as shown in Fig. 4(c). The Nyquist plots for the BiVO₄ and Co–Pi/BiVO₄ photoanodes are fitted to the equivalent circuit (depicted in the inset) for comparative analysis of the charge transfer resistance at the SEI. After the incorporation of Co–Pi onto the BiVO₄ photoanode, the charge transfer resistance (R_{ct}) decreases dramatically from 7.88 kΩ for the BiVO₄ to 0.73 kΩ for the Co–Pi/BiVO₄ photoanode. This substantial reduction indicates a notable improvement in mitigating the surface state recombination by Co–Pi. The markedly lower R_{ct} for the Co–Pi/BiVO₄ photoanode further corroborates that Co–Pi can effectively passivate surface states, thereby extending the lifetime of photogenerated holes engaged in the water oxidation process. Figure 4(d) shows the Mott-Schottky plots for the BiVO₄ and Co–Pi/BiVO₄ photoanodes. The presence of a distinct positive slope in the linear part of the plots indicates the manifestation of *n*-type

characteristics of the photoanode films. The donor density, calculated from the Mott-Schottky slope, is $N_d = 5.4 \times 10^{20} \text{ cm}^{-3}$ and $14.3 \times 10^{20} \text{ cm}^{-3}$ for BiVO_4 and Co-Pi/BiVO_4 , respectively. These values demonstrate an order of magnitude higher than similar BiVO_4 photoanodes prepared by direct deposition.³³⁻³⁵ After Co-Pi passivation on the BiVO_4 electrode, a noticeable cathodic shift in the flat-band potential (E_{fb}) is observed, with its value decreasing from $0.68 \text{ V}_{\text{RHE}}$ to $0.47 \text{ V}_{\text{RHE}}$. This large cathodic shift of $-0.21 \text{ V}_{\text{RHE}}$ is highly advantageous as it promotes the flow of electrons across the circuit toward the counter electrode, and as a result, this leads to a reduction in the onset potential for anodic photocurrent.³⁶

Conclusion

Our study introduces a new approach for producing continuous, nanostructured BiVO_4 films for enhanced PEC water oxidation in hydrogen production. This approach involves intercalating V ions into a sputtered Bi_2O_3 film through a gradual annealing process. The optimized BiVO_4 photoanode, with a thickness of 270 nm, exhibits outstanding PEC performance with a strong, robust photocurrent density of 1.0 mA/cm^2 at $1.23 \text{ V}_{\text{RHE}}$ in a neutral electrolyte, notably without the necessity for a hole scavenger. This performance ranks among the best recorded for uncatalyzed BiVO_4 photoanodes measured under comparable conditions. The absence of pinholes in our intercalated BiVO_4 film effectively suppresses solution-mediated recombination at FTO regions exposed to the electrolyte, thus increasing the availability of photogenerated holes for water oxidation. Furthermore, the addition of the Co-Pi co-catalyst to the BiVO_4 photoanode facilitates the passivation of surface defects, enhancing the hole lifetime by a remarkable 9-fold. This enhancement results in an exceptional photocurrent of 2.9 mA/cm^2 at $1.23 \text{ V}_{\text{RHE}}$ under standard illumination conditions.

Acknowledgments

The authors would like to acknowledge the support provided by the Center of Hydrogen and energy storage (HES) and the Deanship of Scientific Research (DSR) at King Fahd University of Petroleum & Minerals (KFUPM) for funding this work through project No# DF181021. This work was supported under Australian Research Council (ARC) Discovery Project funding scheme (project DP210101146).

Supplementary data

Supplementary data to this paper can be found online at xxx.

References

1. Qian, Q.; Zhu, Y.; Ahmad, N.; Feng, Y.; Zhang, H.; Cheng, M.; Liu, H.; Xiao, C.; Zhang, G.; Xie, Y., Recent Advancements in Electrochemical Hydrogen Production via Hybrid Water Splitting. *Advanced Materials* **2024**, *36* (4), 2306108.
2. Rahman, M. Z.; Raziq, F.; Zhang, H.; Gascon, J., Key strategies for enhancing H₂ production in transition metal oxide based photocatalysts. *Angewandte Chemie* **2023**, *135* (48), e202305385.
3. Salih, A. K.; Phillips, M. R.; Ton-That, C., Enhanced solar-driven water splitting performance using oxygen vacancy rich ZnO photoanodes. *Solar Energy Materials and Solar Cells* **2023**, *259*, 112436.
4. Zhang, B.; Yu, S.; Dai, Y.; Huang, X.; Chou, L.; Lu, G.; Dong, G.; Bi, Y., Nitrogen-incorporation activates NiFeO_x catalysts for efficiently boosting oxygen evolution activity and stability of BiVO₄ photoanodes. *Nature Communications* **2021**, *12* (1), 6969.
5. Kim, J. H.; Lee, J. S., Elaborately modified BiVO₄ photoanodes for solar water splitting. *Advanced Materials* **2019**, *31* (20), 1806938.
6. Pylarinou, M.; Sakellis, E.; Tsipas, P.; Romanos, G. E.; Gardelis, S.; Dimoulas, A.; Likodimos, V., Mo-BiVO₄/Ca-BiVO₄ homojunction nanostructure-based inverse opals for photoelectrocatalytic pharmaceutical degradation under visible light. *ACS Applied Nano Materials* **2023**, *6* (8), 6759-6771.
7. Wang, L.; Wu, F.; Chen, X.; Ren, J.; Lu, X.; Yang, P.; Xie, J., Defective Metal–Organic framework assisted with nitrogen doping enhances the photoelectrochemical performance of BiVO₄. *ACS Applied Energy Materials* **2021**, *4* (11), 13199-13207.
8. Correa, A. S.; Rabelo, L. G.; Rosa, W. S.; Khan, N.; Krishnamurthy, S.; Khan, S.; Gonçalves, R. V., Interfacial band alignment and photoelectrochemical properties of all-sputtered BiVO₄/FeNiO_x and BiVO₄/FeMnO_xp–n heterojunctions. *Energy Advances* **2023**, *2* (1), 123-136.
9. Gutkowski, R.; Khare, C.; Conzuelo, F.; Kayran, Y.; Ludwig, A.; Schuhmann, W., Unraveling compositional effects on the light-induced oxygen evolution in Bi (V–Mo–X) O₄ material libraries. *Energy & Environmental Science* **2017**, *10* (5), 1213-1221.
10. Rosa, W. S.; Rabelo, L. G.; Tiveron Zampaulo, L. G.; Gonçalves, R. V., Ternary Oxide CuWO₄/BiVO₄/FeCoO_x Films for Photoelectrochemical Water Oxidation: Insights into the Electronic Structure and Interfacial Band Alignment. *ACS Applied Materials & Interfaces* **2022**, *14* (20), 22858-22869.
11. Zhong, D. K.; Choi, S.; Gamelin, D. R., Near-complete suppression of surface recombination in solar photoelectrolysis by "Co-Pi" catalyst-modified W: BiVO₄. *Journal of the American Chemical Society* **2011**, *133* (45), 18370-18377.

12. Liang, Y.; Tsubota, T.; Mooij, L. P.; van de Krol, R., Highly improved quantum efficiencies for thin film BiVO₄ photoanodes. *The Journal of Physical Chemistry C* **2011**, *115* (35), 17594-17598.
13. Choi, S. K.; Choi, W.; Park, H., Solar water oxidation using nickel-borate coupled BiVO₄ photoelectrodes. *Physical chemistry chemical physics* **2013**, *15* (17), 6499-6507.
14. Alarcón-Lladó, E.; Chen, L.; Hettick, M.; Mashouf, N.; Lin, Y.; Javey, A.; Ager, J. W., BiVO₄ thin film photoanodes grown by chemical vapor deposition. *Physical Chemistry Chemical Physics* **2014**, *16* (4), 1651-1657.
15. Eisenberg, D.; Ahn, H. S.; Bard, A. J., Enhanced photoelectrochemical water oxidation on bismuth vanadate by electrodeposition of amorphous titanium dioxide. *Journal of the American Chemical Society* **2014**, *136* (40), 14011-14014.
16. Li, Z.; Feng, J.; Yan, S.; Zou, Z., Solar fuel production: Strategies and new opportunities with nanostructures. *Nano Today* **2015**, *10* (4), 468-486.
17. Sengupta, P.; Shinde, S.; Majumdar, P.; Löffler, M.; Datta, P.; Patra, S., Direct growth of bismuth vanadate thin film arrays on FTO via galvanic deposition mediated by BiOI nanosheets for fabrication of photoelectrochemical non-enzymatic dopamine sensing platform. *Journal of The Electrochemical Society* **2020**, *167* (4), 047513.
18. Polo, A.; Grigioni, I.; Magni, M.; Facibeni, A.; Dozzi, M. V.; Selli, E., Unravelling the bulk and interfacial charge transfer effects of molybdenum doping in BiVO₄ photoanodes. *Applied Surface Science* **2021**, *556*, 149759.
19. Hong, S.; Lee, S.; Jang, J.; Lee, J., Composite Electrodes of BiVO₄ and WO₃ for Enhanced Photoactivity of Water Oxidation. *Energy Env. Sci* **2011**, *4*, 1781.
20. Bi, Y.; Yang, Y.; Shi, X.-L.; Feng, L.; Hou, X.; Ye, X.; Zhang, L.; Suo, G.; Chen, J.; Chen, Z.-G., Bi₂O₃/BiVO₄@graphene oxide van der Waals heterostructures with enhanced photocatalytic activity toward oxygen generation. *Journal of Colloid and Interface Science* **2021**, *593*, 196-203.
21. Wang, L.; Zhang, Y.; Li, W.; Wang, L., Recent advances in elaborate interface regulation of BiVO₄ photoanode for photoelectrochemical water splitting. *Materials Reports: Energy* **2023**, 100232.
22. Cui, J.-Y.; Zhu, S.-S.; Zou, Y.; Zhang, Y.; Yuan, S.-Y.; Li, T.-T.; Guo, S.-Y.; Liu, H.; Wang, J.-J., Improved Photoelectrochemical Performance of BiVO₄ for Water Oxidation Enabled by the Integration of the Ni@ NiO Core–Shell Structure. *Catalysts* **2022**, *12* (11), 1456.
23. Shewale, P.; Agawane, G.; Shin, S.; Moholkar, A.; Lee, J.; Kim, J.; Uplane, M., Thickness dependent H₂S sensing properties of nanocrystalline ZnO thin films derived by advanced spray pyrolysis. *Sensors and Actuators B: Chemical* **2013**, *177*, 695-702.
24. Bhat, S. S.; Jang, H. W., Recent advances in bismuth-based nanomaterials for photoelectrochemical water splitting. *ChemSusChem* **2017**, *10* (15), 3001-3018.

25. Liu, X.; Zhou, H.; Pei, S.; Xie, S.; You, S., Oxygen-deficient WO_{3-x} nanoplate array film photoanode for efficient photoelectrocatalytic water decontamination. *Chemical Engineering Journal* **2020**, *381*, 122740.
26. Mohamedkhair, A. K.; Drmosh, Q. A.; Qamar, M.; Yamani, Z. H., Tuning Structural Properties of WO_3 Thin Films for Photoelectrocatalytic Water Oxidation. *Catalysts* **2021**, *11* (3), 381.
27. Seabold, J. A.; Choi, K.-S., Efficient and stable photo-oxidation of water by a bismuth vanadate photoanode coupled with an iron oxyhydroxide oxygen evolution catalyst. *Journal of the American Chemical Society* **2012**, *134* (4), 2186-2192.
28. Jahangir, T. N.; Khan, A. Z.; Kandiel, T. A.; El Ali, B. M., Insights into the charge transfer kinetics in BiVO_4 photoanodes modified with transition metal-based oxygen evolution electrocatalysts. *Catalysis Today* **2023**, *413*, 113918.
29. Kalanur, S. S.; Seo, H., An experimental and density functional theory studies of Nb-doped BiVO_4 photoanodes for enhanced solar water splitting. *Journal of Catalysis* **2022**, *410*, 144-155.
30. Eftekharinia, B.; Moshaii, A.; Dabirian, A.; Vayghan, N. S., Optimization of charge transport in a Co-Pi modified hematite thin film produced by scalable electron beam evaporation for photoelectrochemical water oxidation. *Journal of materials chemistry A* **2017**, *5* (7), 3412-3424.
31. Khan, I.; Khan, A. Z.; Sufyan, A.; Khan, M. Y.; Basha, S. I.; Khan, A., Ultrasonically controlled growth of monodispersed octahedral BiVO_4 microcrystals for improved photoelectrochemical water oxidation. *Ultrasonics Sonochemistry* **2020**, *68*, 105233.
32. Xiao, J.; Fan, L.; Zhao, F.; Huang, Z.; Zhou, S.-F.; Zhan, G., Kinetic analysis of the synergistic effect of NaBH_4 treatment and Co-Pi coating on Fe_2O_3 photoanodes for photoelectrochemical water oxidation. *Journal of Catalysis* **2020**, *381*, 139-149.
33. Kalanur, S. S.; Lee, Y. J.; Seo, H.; Pollet, B. G., Enhanced photoactivity towards bismuth vanadate water splitting through tantalum doping: An experimental and density functional theory study. *Journal of Colloid and Interface Science* **2023**, *650*, 94-104.
34. Zhang, B.; Zhang, H.; Wang, Z.; Zhang, X.; Qin, X.; Dai, Y.; Liu, Y.; Wang, P.; Li, Y.; Huang, B., Doping strategy to promote the charge separation in BiVO_4 photoanodes. *Applied Catalysis B: Environmental* **2017**, *211*, 258-265.
35. Zhou, C.; Sanders-Bellis, Z.; Smart, T. J.; Zhang, W.; Zhang, L.; Ping, Y.; Liu, M., Interstitial lithium doping in BiVO_4 thin film photoanode for enhanced solar water splitting activity. *Chemistry of Materials* **2020**, *32* (15), 6401-6409.
36. Dey, K. K.; Gahlawat, S.; Ingole, P. P., BiVO_4 optimized to nano-worm morphology for enhanced activity towards photoelectrochemical water splitting. *Journal of Materials Chemistry A* **2019**, *7* (37), 21207-21221.

Supporting Information

Nanostructured BiVO₄ Photoanodes Fabricated by Vanadium-infused Interaction for Efficient Solar Water Splitting

Amar K. Salih^{1,2}, Abdul Zeeshan Khan³, Qasem A. Drmosh⁴, Tarek A. Kandiel^{3,4,*},
Mohammad Qamar⁴, Tahir Naveed Jahangir³, Cuong Ton-That^{1,*}, Zain H. Yamani^{2,4}

¹School of Mathematical and Physical Sciences, University of Technology Sydney, Ultimo,
New South Wales 2007, Australia

²Physics Department, King Fahd University of Petroleum and Minerals, Dhahran, 31261,
Saudi Arabia

³Chemistry Department, King Fahd University of Petroleum and Minerals, Dhahran, 31261,
Saudi Arabia

⁴Center of Hydrogen and Energy Storage (IRC-HES), King Fahd University of Petroleum
and Minerals, Dhahran 31261, Saudi Arabia

*Corresponding authors.

E-mail address: Cuong.Ton-That@uts.edu.au ; tarek.kandiel@kfupm.edu.sa

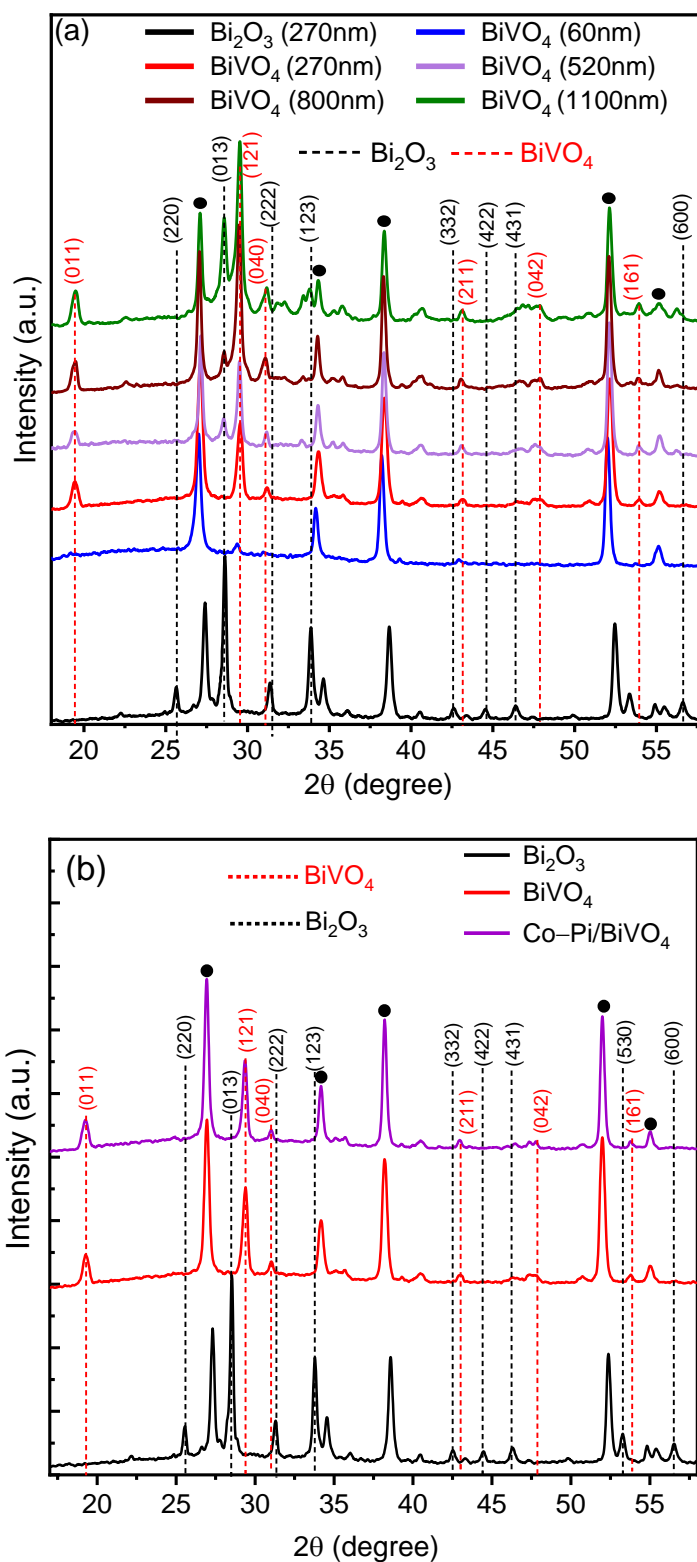


Figure S1. (a) XRD patterns of BiVO₄ films obtained from V intercalation into Bi₂O₃ films with thicknesses ranging from 60 to 1100 nm, and the XRD pattern of the pristine Bi₂O₃ film prior to the V intercalation. Black dots correspond to the FTO substrate, while black and red dashed lines indicate reflections from tetragonal Bi₂O₃ and monoclinic BiVO₄ phases, respectively. The Bi₂O₃ film exhibits dominant XRD peaks corresponding to (220), (013), and

(123) reflections of the tetragonal structure. These Bi_2O_3 peaks completely disappear after V intercalation in the thinner BiVO_4 films (60 and 270 nm thick), revealing a complete phase transformation into a monoclinic BiVO_4 phase. The transformed BiVO_4 films display clearly identifiable peaks (011), (121), (040), (211) and (161) of the monoclinic phase (JCPDS no. 14–0688). However, residual Bi_2O_3 tetragonal phase is detected in the films with thicknesses of 520, 800, and 1100 nm thick films. (b) XRD patterns of the BiVO_4 and Co–Pi/ BiVO_4 films fabricated from a 270 nm thick Bi_2O_3 film, alongside the XRD pattern of tetragonal Bi_2O_3 for comparison. No distinct Co–Pi XRD peaks are observed in the Co–Pi/ BiVO_4 film.

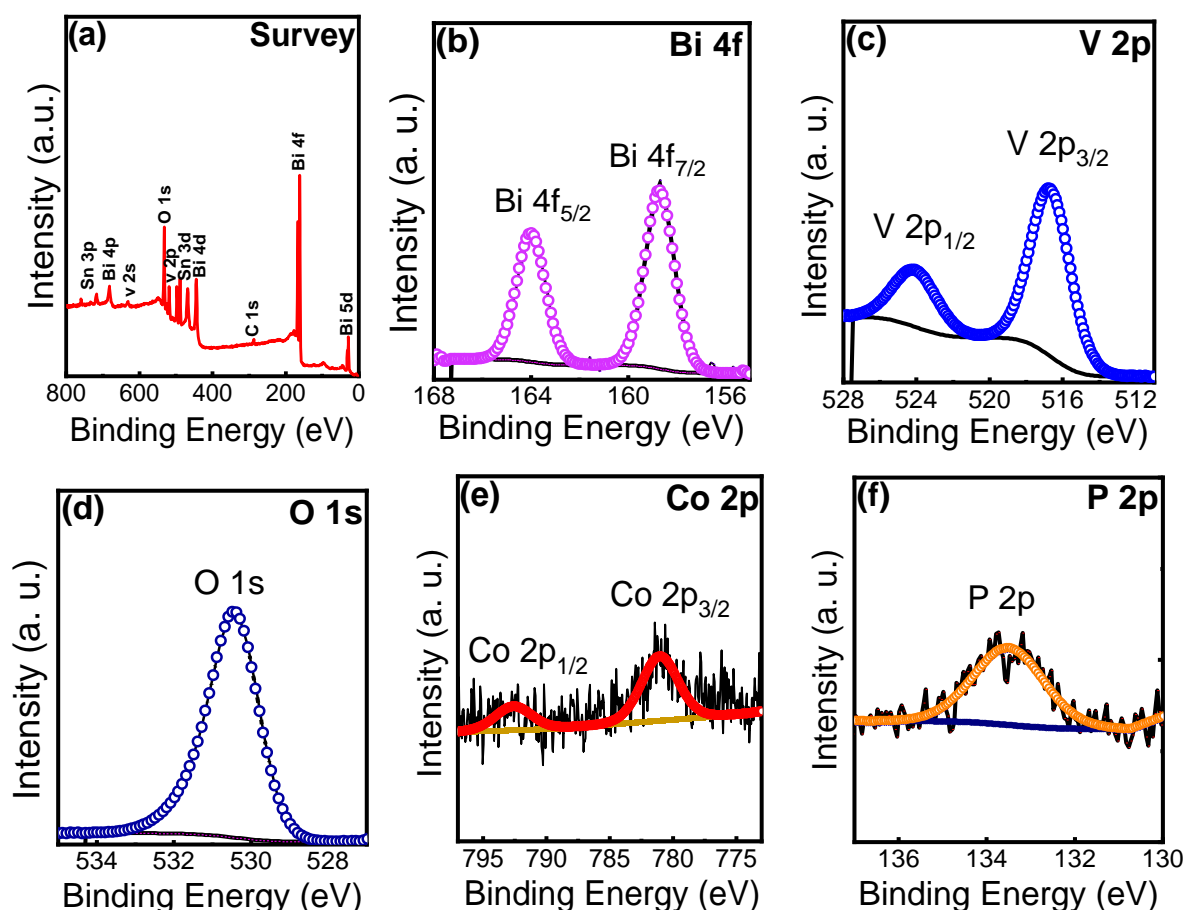


Figure S2. (a) XPS survey spectrum of the 270-nm thick BiVO₄ film after etching by Ar⁺ ions sputtering for 120 seconds. The spectrum reveals photoemission peaks corresponding to Bi, V, and O, as well as an Sn peak arising from the FTO substrate. The presence of the strong V peaks in the XPS spectrum confirms the intercalation of V ions throughout the thickness of the Bi₂O₃ film, extending down to the substrate. (b) XPS Bi 4f peaks showing a binding energy difference of 5.3 eV between Bi 4f_{7/2} and Bi 4f_{5/2} spin-orbit components, providing evidence for the oxidation state of Bi³⁺.¹ (c) XPS V 2p spectrum revealing the V⁵⁺ oxidation state with distinct spin-orbit peaks at 516.7 eV (V 2p_{3/2}) and 524.2 eV (V 2p_{1/2}).¹ (d) XPS O 1s spectrum at 530.4 eV associated with lattice oxygen. For the Co–Pi/BiVO₄ film, the Co–Pi co-catalyst integration on the film surface is confirmed by the presence of (e) Co 2p peaks at 781.1 eV (Co 2p_{3/2}) and 793.2 eV (Co 2p_{1/2}), along with (f) the P 2p peak at 133.4 eV.²

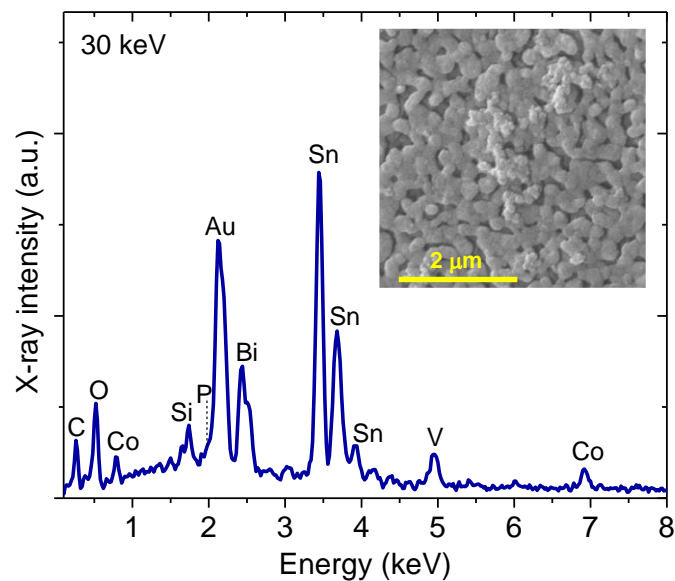


Figure S3. EDX spectrum of the Co–Pi/BiVO₄ film revealing the presence of all the anticipated elements: Bi, V, O, Co and P. The peaks of Sn, Si, and Au arise the FTO glass substrate and the gold coating used for SEM imaging purposes. The SEM image (inset) shows Co-Pi nanoparticles on the BiVO₄ film.

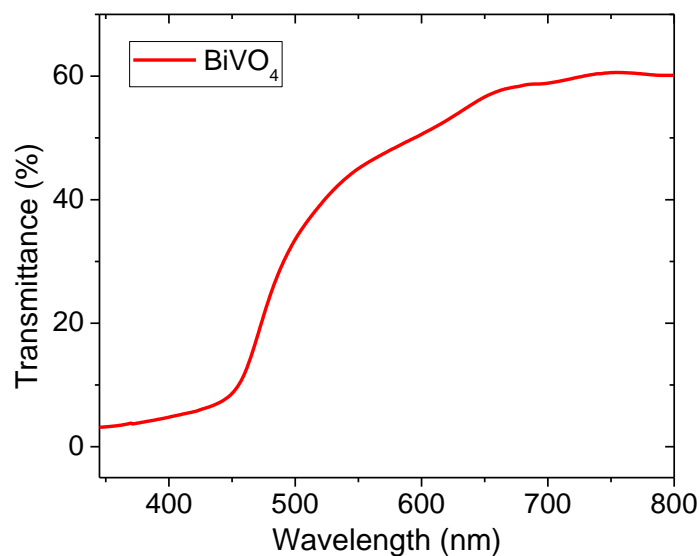


Figure S4. Optical transmission spectrum of the optimized BiVO₄ film showing a transmittance of < 10% for wavelengths below 450 nm and a broad edge that allows this film to absorb well into the visible range.

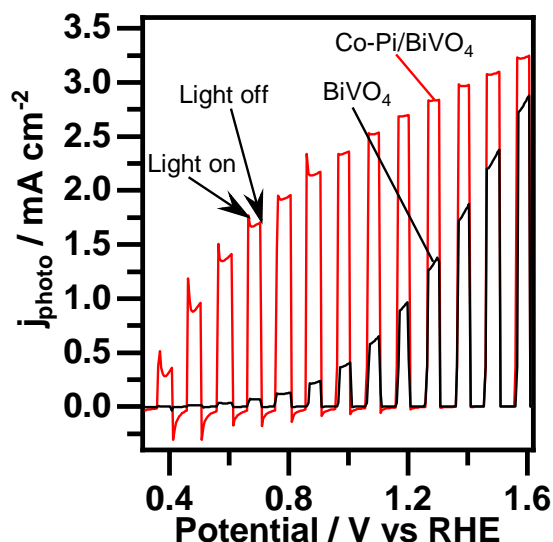


Figure S5. Chopped LSV curves showing the photoelectrochemical water oxidation of the BiVO_4 and Co-Pi/BiVO_4 photoanodes, measured in 0.5 M PBS solution under AM 1.5G illumination. The photocurrent displays a notable enhancement after the integration of Co-Pi co-catalyst, rising from 1.0 mA/cm^2 in the BiVO_4 photoanode to 2.9 mA/cm^2 in the Co-Pi/BiVO_4 configuration at $1.23 \text{ V}_{\text{RHE}}$. The LSV curves exhibit a diminishing trend in anodic spikes with increasing applied potential, attributed to enhanced charge separation at higher potentials.

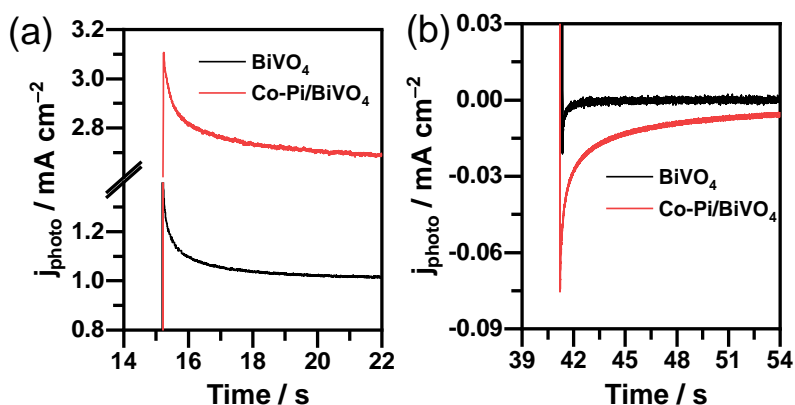


Figure S6. (a) Anodic and (b) Cathodic spikes observed for the BiVO_4 and Co-Pi/BiVO_4 photoanodes during transient photocurrent measurements at $1.23 \text{ V}_{\text{RHE}}$ in 0.5 M PBS solution under AM 1.5G illumination. The photocurrent transient of the Co-Pi/BiVO_4 configuration exhibits a notably heightened cathodic spike when switching off the light, indicating increased hole accumulation at the surface. This result is consistent with the suppression of surface recombination due to the Co-Pi catalyst.

Table S1: Comparison of PEC performance at 1.23 V_{RHE} for BiVO₄ photoanodes in this work and recent reports. To ensure a fair comparison, the table is limited to undoped BiVO₄ photoanodes with and without Co-Pi co-catalysts, measured in a neutral electrolyte and under conditions similar to those employed in this work.

Synthesis method	Electrolyte (pH = 7)	J (mA/cm ²) at 1.23 V _{RHE}		Reference
		No catalyst	Co-Pi co-catalyst	
V intercalation of Bi ₂ O ₃	0.5 M H ₂ KO ₄ P	1.0	2.9	This work
Electrodeposition	0.1 M KPi	0.5	0.8	[3]
Drop-casting	0.5 M H ₂ KO ₄ P	0.4	2.3	[4]
Calcination of Bi ₂ O ₃	0.5 M H ₂ KO ₄ P	2.6	2.9	[5]

References

1. Fang, G.; Liu, Z.; Han, C., Enhancing the PEC water splitting performance of BiVO₄ co-modifying with NiFeOOH and Co-Pi double layer cocatalysts. *Applied Surface Science* **2020**, *515*, 146095.
2. Zhang, Y.; Wang, D.; Zhang, X.; Chen, Y.; Kong, L.; Chen, P.; Wang, Y.; Wang, C.; Wang, L.; Liu, Y., Enhanced photoelectrochemical performance of nanoporous BiVO₄ photoanode by combining surface deposited cobalt-phosphate with hydrogenation treatment. *Electrochimica Acta* **2016**, *195*, 51-58.
3. Yang, L.; Wang, R.; Chu, D.; Chen, Z.; Zhong, F.; Xu, X.; Deng, C.; Yu, H.; Lv, J., BiVO₄ photoelectrodes for unbiased solar water splitting devices enabled by electrodepositing of Cu₂O simultaneously as photoanode and photocathode. *Journal of Alloys and Compounds* **2023**, *945*, 169336.
4. Jahangir, T. N.; Kandiel, T. A.; Mahar, N.; Khan, A. Z.; Al-Saadi, A. A., Exploring the role of Ti₃C₂T_xMXene in photoelectrochemical water splitting over solution-processed BiVO₄ photoanode. *Materials Today Energy* **2024**, *40*, 101469.
5. Ju, S.; Lee, N.; Sung, H.; Son, S.; Kim, N.; Kim, J.; kyu Kim, J.; Lee, H., Nanostructured BiVO₄ obtained by the vanadium calcination of Bi₂O₃ nanohelices for enhanced photoelectrochemical water splitting. *Journal of Materials Chemistry A* **2023**, *11* (33), 17644-17650.